Energy of dendritic avalanches in thin-film superconductors

T. Qureishy, J. I. Vestgården, A. J. Qviller, A. S. Fjellvåg, J. M. Meckbach, A. Torgovkin, T. H. Johansen, K. Ilin, M. Siegel, I. Maasilta, and P. Mikheenko

Citation: AIP Advances **8**, 085128 (2018); doi: 10.1063/1.5045682
View online: https://doi.org/10.1063/1.5045682
View Table of Contents: http://aip.scitation.org/toc/adv/8/8
Published by the American Institute of Physics

Energy of dendritic avalanches in thin-film superconductors

T. Qureishy,[1,a] J. I. Vestgården,[1,2] A. J. Qviller,[3] A. S. Fjellvåg,[4] J. M. Meckbach,[5] A. Torgovkin,[6] T. H. Johansen,[1,7] K. Ilin,[5] M. Siegel,[5] I. Maasilta,[6] and P. Mikheenko[1]

[1]*Department of Physics, University of Oslo, P.O. Box 1048 Blindern, 0316 Oslo, Norway*
[2]*Norwegian Defence Research Establishment (FFI), P.O. Box 25, 2027 Kjeller, Norway*
[3]*nSolution AS, Maries Gate 6, 0368 Oslo, Norway*
[4]*Department of Chemistry, University of Oslo, P.O. Box 1033 Blindern, 0315 Oslo, Norway*
[5]*Institute of Micro- and Nanoelectronic Systems, Karlsruhe Institute of Technology, Hertzstr. 16, 76187 Karlsruhe, Germany*
[6]*Nanoscience Center, Department of Physics, P.O. Box 35, University of Jyväskylä, FIN-40014 Jyväskylä, Finland*
[7]*Institute for Superconducting and Electronic Materials, University of Wollongong, Northfields Avenue, Wollongong, NSW 2522, Australia*

(Received 22 June 2018; accepted 23 August 2018; published online 30 August 2018)

A method for calculating stored magnetic energy in a thin superconducting film based on quantitative magneto-optical imaging is developed. Energy and magnetic moment are determined with these calculations for full hysteresis loops in a thin film of the superconductor NbN. Huge losses in energy are observed when dendritic avalanches occur. Magnetic energy, magnetic moment, sheet current and magnetic flux distributions, all extracted from the same calibrated magneto-optical images, are analyzed and discussed. Dissipated energy and the loss in moment when dendritic avalanches occur are related to each other. Calculating these losses for specific spatially-resolved flux avalanches is a great advantage, because of their unpredictable and non-reproducible nature. The relative losses in energy are much higher than the relative losses in moment. https://doi.org/10.1063/1.5045682

When exposed to an external magnetic field, type-II superconductors are susceptible to flux jumps caused by a thermomagnetic instability.[1] Abrikosov vortices dissipate heat as they move into a superconductor resulting in depinning of other vortices, which, in turn, dissipate more heat and further reduce pinning as they propagate in the sample. Such flux jumps are harmful to the operation of superconducting devices because they introduce noise, heat the superconductor locally, and lower the magnetic moment.[2–9] The spatial flux structure of the flux jumps in films is often branched, complex structures. The residual flux distributions of such dendritic flux avalanches have been mapped using magneto-optical techniques in many materials, such as Nb,[10,11] NbN,[12,13] MgB_2,[14–16] YBCO,[17–19] Nb_3Sn,[20] YNi_2B_2C,[21] and a-MoSi[22] as well as in foils of Nb[23] and MgB_2 tapes.[24] The shape and exact fields at which the avalanches occur are non-reproducible, and they propagate at speeds of several kilometers per second.[18,19]

It has been found that such avalanches can be prevented by a metal layer covering all or parts of the superconductor,[25–28] or by a thorough adjustment of films morphology at nano-scale.[13] If not prevented, avalanches can be highly energetic and even permanently damage the sample.[29] Overheating and destruction of superconductors caused by thermomagnetic avalanches is a result of sudden release of large amounts of energy stored in the magnetic field.

[a]Corresponding author. E-mail: thomashq@uio.no

The avalanche phenomenon is a consequence of meta-stability of the critical state.[30] Iwasa et al.[31] have measured the energy released when flux jumps occur in Nb-Ti superconducting wires by observing the volume of evaporated liquid helium during the jump event. In the present work we use magneto-optical imaging (MOI) to measure both the energy built up during a field ramp, and the amount of magnetic energy released when dendritic avalanches occur in a thin superconducting NbN film.

The energy of the magnetic field is given by $U = \frac{1}{2}\int \mathbf{B}\cdot\ \mathbf{H}d^3r$, where for a thin superconductor film at low fields $\mathbf{B} \approx \mu_0\mathbf{H}$. The integration over all space surrounding the sample is inconvenient and so we use the equivalent formula:

$$U = \frac{1}{2}\int \mathbf{j}\cdot\mathbf{A}d^2r, \tag{1}$$

where $\mathbf{j}$ is the sheet current and $\mathbf{A}$ is the magnetic vector potential. When the perpendicular component of the magnetic field, H_z, is known in a sufficiently large region in the sample plane, the sheet current can be efficiently calculated in Fourier space as:[32]

$$\tilde{j}_{x,y} = \pm i\tilde{H}_z 2k_{y,x}/k, \tag{2}$$

where k_x, k_y and $k = \sqrt{k_x^2 + k_y^2}$ are Fourier space wave-vectors, and $\tilde{H}_z$ and $\tilde{j}_{x,y}$ are magnetic field and sheet current in Fourier space, respectively. Provided that the magnetic field is generated from a thin-film current, the Coulomb gauge magnetic vector potential components have equally simple formulations in Fourier space (see supplementary material):

$$\tilde{A}_{x,y} = \pm i\mu_0\tilde{H}_z k_{y,x}/k^2, \tag{3}$$

Then, by Eq. (1) the energy of the magnetic field can be calculated from H_z in the film plane. Such H_z distributions can be mapped by quantitative MOI.

Magneto-optical imaging is a technique in which magnetic flux is visualized in a material using the Faraday effect.[33] Light is first sent through a polarizer, and the resulting polarized light is thereafter projected upon a Faraday-rotating indicator film lying on top of the sample, which is mounted on a cold finger in a liquid helium cryostat. Inside the indicator film, the incident light undergoes a Faraday rotation corresponding to the local magnetic field strength. It is then reflected by a mirror layer on the side of the indicator facing the sample, undergoes another equivalent Faraday rotation and leaves the film going through a crossed analyzer of an optical microscope. In this polarizer-analyzer configuration and for our range of applied magnetic fields, the light intensity I in the MO images is a monotonic function of H_z, thus the inverse function also exists. Magnetic field is applied from coils connected to a power supply. Quantitative images of the magnetic flux distribution can be obtained by calibrating MO images above the critical temperature (T_c) of the superconductor. Then I is measured below T_c and used to determine H_z in the plane of the superconductor. This calibration procedure avoids the problem of inhomogeneous incident light and the non-linear response of the indicator film. In this way, MO images are transformed into exact maps of magnetic field perpendicular to the plane of the film, $\mu_0 H_z$.[33–37] The quantitative map of H_z enables us to calculate $\mathbf{j}$ by Eq. (2), $\mathbf{A}$ by Eq. (3) and then U from Eq. (1). The calculation of $\mathbf{j}$ can be improved by correcting for in-plane magnetic fields. However, such a correction was not made, because this effect is less pronounced at low fields at which the measurements were done.[34] The magnetic moment, m, is calculated as $m = \int g d^2r$ where the local magnetization, g, is calculated in Fourier space as $\tilde{g} = \tilde{H}_z 2/k$. A fine mesh with discretization size 5.15x5.15 μm^2 was used in all calculations.

The technique was tested on a 420 nm thick NbN film deposited by reactive magnetron sputtering onto a heated 10×10 mm^2 MgO[100] substrate.[38] Extra lateral material from the sample was removed by reactive ion etching to create four smaller square samples with smooth edges on top of the substrate. After that, the substrate was cut into four pieces by laser cutting, each with one film with an area of approximately 4x4 mm^2 on top. The present work describes results for one of these samples, with dimensions 4.13x4.02 mm^2. The Faraday-active indicator film was an in-plane magnetized bismuth-substituted ferrite garnet film deposited by liquid phase epitaxy on a gadolinium gallium garnet substrate with an aluminum mirror.[39]

Fig. 1 shows quantitative MO images of the film before and after a dendritic avalanche occurs. The sample was zero-field cooled to 3.5 K before applying the field. In Fig. 1(a), obtained at $\mu_0 H_a$ = 13.6 mT, flux has gradually penetrated into the superconductor from the edges and formed critical state-like regions. In Fig. 1(b), which was obtained at $\mu_0 H_a$ = 14.0 mT, a dendritic avalanche has appeared. Also there are thin dark lines at the sample edges, most visible on the left edge. This is a result of current inversion in these areas. Close to the sample boundaries, the current flows in the opposite direction. This leads to an opposite gradient and decrease of the absolute value of $\mu_0 H_z$.

Fig. 2 shows a magnetic moment loop calculated from 255 MO images obtained at 5.0 K (black line). The five parts of the loop are numbered. At every applied field the magnetic moment is calculated from a quantitative MO image. This loop has a flux jump in the third (0 to −21.25 mT) and fifth (0 to 21.25 mT) parts. For comparison, Fig. 2 also shows m obtained from dc magnetometry (red line) using a Physical Properties Measurement System (PPMS). There is good agreement between m obtained by these two techniques in the first and second parts of the loop, which demonstrates good accuracy of the calibration procedure. The lack of overlapping in the fourth part is caused by the very strong flux jumps in the third part of the loop in DCM. The figure reveals that more flux jumps took place during the magnetometry measurement compared to MOI. This is presumably because the film's substrate was firmly attached to a cold finger in MOI, thereby having improved heat removal from the sample.[16]

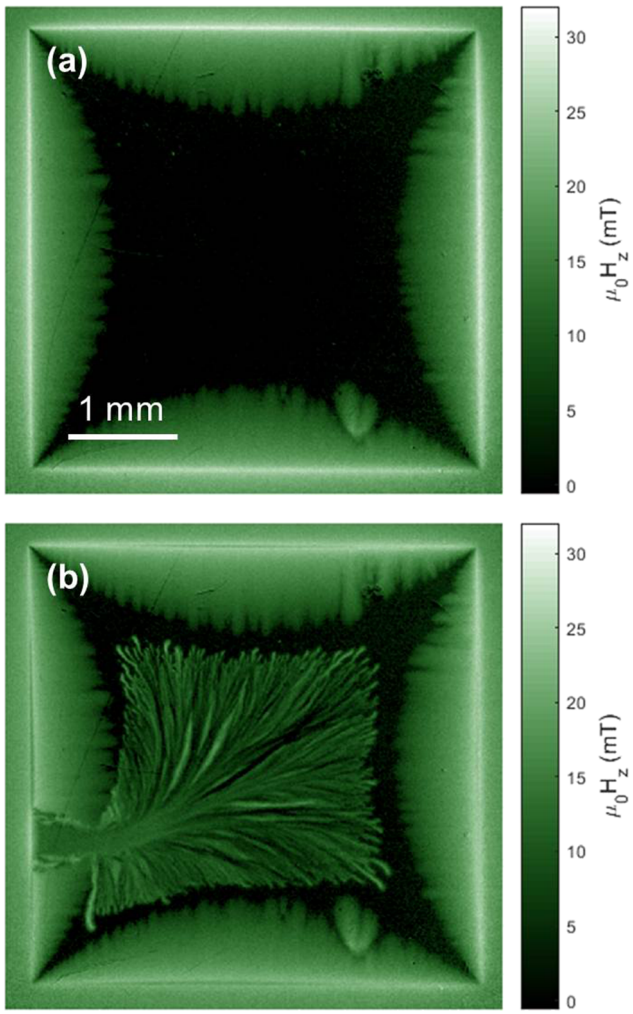

FIG. 1. Quantitative MO images in the film before (a) and after (b) a dendritic avalanche occurred, obtained at 13.6 and 14.0 mT, respectively. The film was zero-field cooled to 3.5 K before applying the magnetic field.

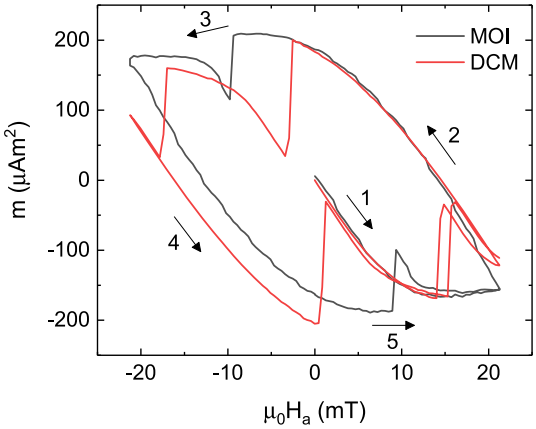

FIG. 2. A full magnetic moment loop, calculated from quantitative MO images (MOI, black) and measured with dc magnetometry (DCM, red). In both cases, the film was zero-field cooled to 5.0 K, and the magnetic field was first increased to 21.25 mT, then decreased back to zero, applied in the opposite direction to −21.25 mT, decreased back to zero, and finally increased again to 21.25 mT.

Fig. 3 shows a part of the magnetic moment virgin curve (first part of the loop) calculated from MO images obtained at 3.5 K (black solid line). The magnitude of negative m increases when a field $\mu_0 H_a$ is applied. At $\mu_0 H_a$ = 13.6 mT, the absolute value of m abruptly decreases from 211 to 135 μAm^2, corresponding to a loss of 36% of the moment. After this flux jump, which is visualized in Fig. 1(b), the magnitude of m continues to increase until it saturates, before starting to decrease slowly. The decrease is caused by a magnetic field-dependence of the critical current density, $J_c(B)$. Shown in Fig. 3 is also the magnetic energy U as a function of $\mu_0 H_a$ (blue dashed line), calculated from the same MO images. The energy increases with $\mu_0 H_a$. At $\mu_0 H_a$ = 13.6 mT, i.e. the field at which m suddenly changed, U abruptly decreases from 0.921 to 0.386 μJ, which means that 58% of U had dissipated. Hence, the relative decrease in U during the flux jump is greater than the relative decrease in m. After the flux jump, U continues to increase, then it saturates, and finally starts to decrease. The relative decrease in magnitude of U after saturation is also greater than that of m.

Presented in Fig. 4 are maps of spatially resolved sheet current $j = |\mathbf{j}|$ in the sample before and after the flux jump. $\mathbf{j}$ was calculated from Eq. (2). The images were created by inversion of the H_z

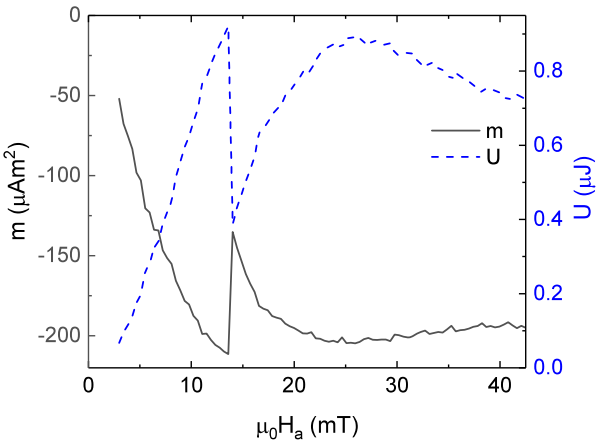

FIG. 3. Magnetic moment m (black solid line) and stored magnetic energy U (blue dashed line) as functions of applied magnetic field $\mu_0 H_a$, calculated from quantitative MO images. The magnetic field was applied after zero-field cooling the sample to 3.5 K. A flux jump occurred at 13.6 mT, resulting in a decrease in negative moment from −211 to −135 μAm^2 and a decrease of U from 0.921 to 0.386 μJ. This flux jump is visualized in Figs. 1 and 4.

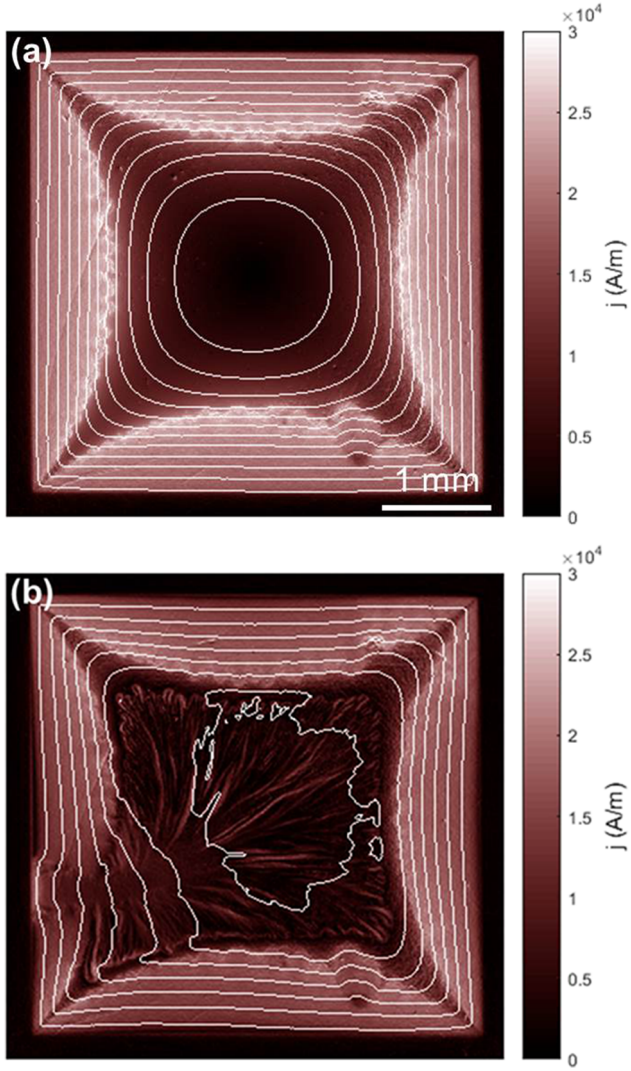

FIG. 4. Sheet current j in the film before (a) and after (b) the avalanche, calculated from quantitative MO images presented in Figs. 1(a) and (b), respectively. The field was applied after zero-field cooling the film to 3.5 K. The applied fields in (a) and (b) are 13.6 and 14.0 mT, respectively. Current streamlines are plotted as contour lines of g.

maps in Fig. 1. The area of the map used in the calculations was 5.55x5.08 mm^2, so that $\mu_0 H_z$ in an area covering at least half a millimeter outside each sample edge was used in the inversion procedure. Current streamlines are plotted as contour lines of g. In Fig. 4(a), j is higher in the area penetrated with magnetic flux than in the flux-free region. The region without magnetic flux has, however, a finite j, which decreases farther into the film and reaches zero at a point in the centre of the sample. This is a common behavior for superconducting thin films.[40] Before the avalanche, the current streamlines are rounded in the flux-free area and parallel to the sample edges in the flux penetrated regions, but j increases from the edges to the flux fronts. This is because the critical current density is H-dependent, and in this case it fits reasonably well Kim's model,[41] $J_c = J_{c0}/(1 + H_z/H_{z0})$ with $\mu_0 H_{z0} = 31$ mT and $J_{c0} = 7.4{\cdot}10^{10}$ Am^{-2}. The jump in Fig. 4(b) is in the form of a dendritic avalanche. The enhanced current at the avalanche root at the left edge in Fig. 4(b) is a critical state-like shielding of the flux in the avalanche stem, c.f. Fig. 1(b). During the avalanche, energy is dissipated as Joule heating in the core of the branches. Yet, also the overall magnitude of current in the critical-state region is significantly reduced after the avalanche, making the current subcritical.

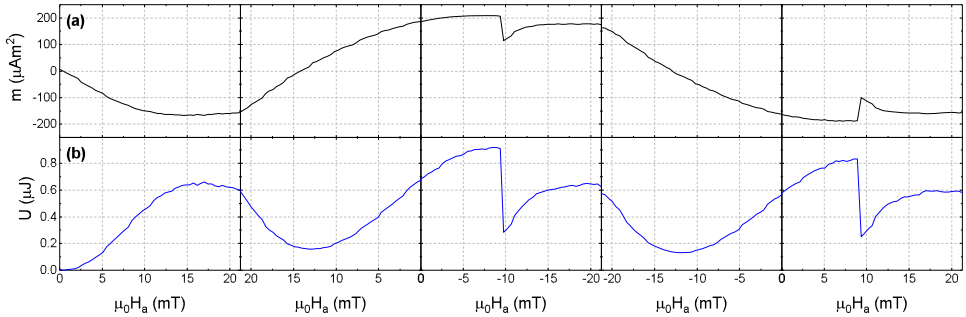

FIG. 5. (a) Magnetic moment m as a function of applied field for a full loop at 5.0 K, calculated from MO images. The same data was used in Fig. 2, but here the five parts of the loop are plotted in series. (b) Magnetic energy U as a function of applied field calculated from the same MO images.

Fig. 5(a) shows m as a function of $\mu_0 H_a$ found from quantitative MO images for the same loop as presented in Fig. 2, but with the five parts plotted in consecutive graphs. A jump in m due to a dendritic avalanche is observed in the third and fifth parts. More importantly, Fig. 5(b) shows U calculated from the same MO images. The sudden decrease in energy occurs at the same fields as the fields at which m is lowered, but the relative amount of dissipated energy is higher than the relative amount of lost moment.

In order to find a relation between losses in U and m, flux jumps in several loops were investigated. Fig. 6 shows a plot of dissipated energy during an avalanche, ΔU, as a function of moment lost during the same avalanche, Δm, for all avalanches observed in several loops. Each point corresponds to one avalanche, and the data were collected from three full loops obtained at 3.5 K, one at 4.0 K, three at 5.0 K and three at 6.0 K. The average values of Δm and ΔU are 89.2 μAm^2 and 0.600 μJ, respectively. The data in Fig. 6 are plotted with a proportional fit $\Delta U = 6.71 \cdot 10^{-3}$ J(Am^2)$^{-1}\Delta m$, with a standard deviation of $1.90 \cdot 10^{-2}\mu$J corresponding to a 95% confidence interval. Following these results, losses in energy caused by thermomagnetic avalanches can be estimated from magnetometry. The evolution of avalanches on the NbN film is too fast to be mapped by our quantitative MOI. However, assuming that the main characteristics are similar to YBCO, the evolution takes place on a time scale of $\Delta t \sim 100$ ns.[18,19] This means that the average dissipation rate, $\Delta U/\Delta t$, is on the order a few Watts.

To conclude, we have calculated magnetic moment and magnetic energy from magneto-optical images and also losses in moment and energy when dendritic avalanches occur. We have characterized a superconducting film by magneto-optical imaging, and observed flux jumps in the form of dendritic

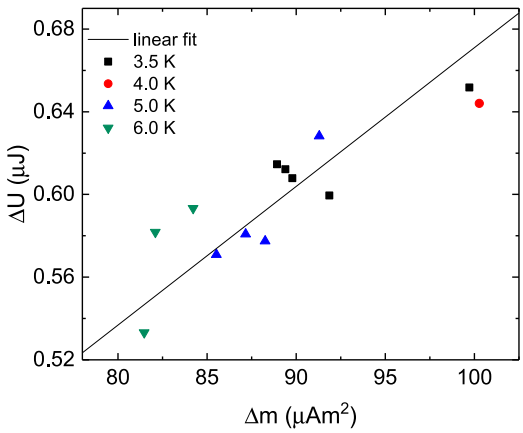

FIG. 6. Dissipated energy ΔU as a function of decrease in magnetic moment Δm for the dendritic avalanches observed in several experiments. The straight line is a proportional fit.

avalanches. Spatially resolved images of sheet current have been calculated, both before and after a dendritic avalanche. Furthermore, magnetic moment and magnetic energy as a function of applied magnetic field have been calculated for full moment loops, allowing to find the change in moment and dissipated energy for specific spatially-resolved dendritic avalanches. Dissipated energy was shown to be proportional to loss in moment by fitting. We have found that relative losses in energy are higher than losses in moment, which emphasizes the importance of preventing the occurrence of dendritic avalanches in applications of superconducting films, especially those that use stored magnetic energy.

See supplementary material for a detailed description of calculating the magnetic vector potential **A**.

The authors thank S. Kumar for assistance with dc magnetometry measurements. The Research Council of Norway is acknowledged for the support to the Norwegian Micro- and Nano-Fabrication Facility, NorFab (197411/V30), as is the Academy of Finland (Project no. 298667).

[1] R. G. Mints and A. L. Rakhmanov, Rev. Mod. Phys. **53**, 551 (1981).
[2] S. Jin, H. Mavoori, C. Bower, and R. B. van Dover, Nature **411**, 563 (2001).
[3] S. X. Dou, X. L. Wang, J. Horvat, D. Milliken, A. H. Li, K. Konstantinov, E. W. Collings, M. D. Sumption, and H. K. Liu, Phys. C **361**, 79 (2001).
[4] X. L. Wang, S. Soltanian, J. Horvat, A. H. Liu, M. J. Qin, H. K. Liu, and S. X. Dou, Phys. C **361**, 149 (2001).
[5] Z. W. Zhao, S. L. Li, Y. M. Ni, H. P. Yang, Z. Y. Liu, H. H. Wen, W. N. Kang, H. J. Kim, E. M. Choi, and S. I. Lee, Phys. Rev. B **65**, 064512 (2002).
[6] A. Gümbel, J. Eckert, G. Fuchs, K. Nenkov, K.-H. Müller, and L. Schultz, Appl. Phys. Lett. **80**, 2725 (2002).
[7] Y. Kimishima, S. Takami, T. Okuda, M. Uehara, T. Kuramoto, and Y. Sugiyama, Phys. C **463-465**, 281 (2007).
[8] E. Yanmaz, B. Şavaşkan, M. Başoğlu, E. Taylan Koparan, N. R. Dilley, and C. R. M. Grovenor, J. Alloy. Compd. **480**, 203 (2009).
[9] M. Motta, F. Colauto, W. A. Ortiz, J. Fritzsche, J. Cuppens, W. Gillijns, V. V. Moshchalkov, T. H. Johansen, A. Sanchez, and A. V. Silhanek, Appl. Phys. Lett. **102**, 212601 (2013).
[10] C. A. Durán, P. L. Gammel, R. E. Miller, and D. J. Bishop, Phys. Rev. B **52**, 75 (1995).
[11] E. Altshuler, T. H. Johansen, Y. Paltiel, P. Jin, K. E. Bassler, O. Ramos, Q. Y. Chen, G. F. Reiter, E. Zeldov, and C. W. Chu, Phys. Rev. B **70**, 140505 (2004).
[12] I. A. Rudnev, D. V. Shantsev, T. H. Johansen, and A. E. Primenko, Appl. Phys. Lett. **87**, 042502 (2005).
[13] V. V. Yurchenko, K. Ilin, J. M. Meckbach, M. Siegel, A. J. Qviller, Y. M. Galperin, and T. H. Johansen, Appl. Phys. Lett. **102**, 252601 (2013).
[14] T. H. Johansen, M. Baziljevich, D. V. Shantsev, P. E. Goa, Y. M. Galperin, W. N. Kang, H. J. Kim, E. M. Choi, M.-S. Kim, and S. I. Lee, Supercond. Sci. Technol. **14**, 726 (2001).
[15] J. Albrecht, A. T. Matveev, J. Strempfer, H.-U. Habermeier, D. V. Shantsev, Y. M. Galperin, and T. H. Johansen, Phys. Rev. Lett. **98**, 117001 (2007).
[16] F. Colauto, E. M. Choi, J. Y. Lee, S. I. Lee, V. V. Yurchenko, T. H. Johansen, and W. A. Ortiz, Supercond. Sci. Technol. **20**, L48 (2007).
[17] P. Brüll, D. Kirchgässner, P. Leiderer, P. Berberich, and H. Kinder, Ann. Phys. **504**, 243 (1992).
[18] P. Leiderer, J. Boneberg, P. Brüll, V. Bujok, and S. Herminghaus, Phys. Rev. Lett. **71**, 2646 (1993).
[19] U. Bolz, B. Biehler, D. Schmidt, B.-U. Runge, and P. Leiderer, Europhys. Lett. **64**, 517 (2003).
[20] I. A. Rudnev, S. V. Antonenko, D. V. Shantsev, T. H. Johansen, and A. E. Primenko, Cryogenics **43**, 663 (2003).
[21] S. C. Wimbush, B. Holzapfel, and Ch. Jooss, J. Appl. Phys. **96**, 3589 (2004).
[22] F. Colauto, M. Motta, A. Palau, M. G. Blamire, T. H. Johansen, and W. A. Ortiz, IEEE Trans. Appl. Supercond. **25**, 1 (2015).
[23] M. R. Wertheimer and J. le G. Gilchrist, J. Phys. Chem. Solids **28**, 2509 (1967).
[24] T. Qureishy, C. Laliena, E. Martínez, A. J. Qviller, J. I. Vestgården, T. H. Johansen, R. Navarro, and P. Mikheenko, Supercond. Sci. Technol **30**, 125005 (2017).
[25] M. Baziljevich, A. V. Bobyl, D. V. Shantsev, E. Altshuler, T. H. Johansen, and S. I. Lee, Phys. C **369**, 93 (2002).
[26] E.-M. Choi, H.-S. Lee, H. J. Kim, B. Kang, S.-I. Lee, A. A. F. Olsen, D. V. Shantsev, and T. H. Johansen, Appl. Phys. Lett. **87**, 152501 (2005).
[27] E.-M. Choi, V. V. Yurchenko, T. H. Johansen, H.-S. Lee, J. Y. Lee, W. N. Kang, and S.-I. Lee, Supercond. Sci. Technol. **22**, 015011 (2009).
[28] F. Colauto, E. Choi, J. Y. Lee, S. I. Lee, E. J. Patiño, M. G. Blamire, T. H. Johansen, and W. A. Ortiz, Appl. Phys. Lett. **96**, 092512 (2010).
[29] M. Baziljevich, E. Baruch-El, T. H. Johansen, and Y. Yeshurun, Appl. Phys. Lett. **105**, 012602 (2014).
[30] C. P. Bean, Rev. Mod. Phys. **36**, 31 (1964).
[31] Y. Iwasa, D. B. Montgomery, and H. W. Polzer, J. Appl. Phys. **41**, 2476 (1970).
[32] Ch. Jooss, R. Warthmann, A. Forkl, and H. Kronmüller, Phys. C **299**, 215 (1998).
[33] Ch. Jooss, J. Albrecht, H. Kuhn, S. Leonhardt, and H. Kronmüller, Rep. Prog. Phys. **65**, 651 (2002).
[34] F. Laviano, D. Botta, A. Chiodoni, R. Gerbaldo, G. Ghigo, L. Gozzelino, S. Zannella, and E. Mezzetti, Supercond. Sci. Technol. **16**, 71 (2003).
[35] L. Gozzelino, F. Laviano, P. Przyslupski, A. Tsarou, A. Wisniewski, D. Botta, R. Gerbaldo, and G. Ghigo, Supercond. Sci. Technol. **19**, S50 (2006).

[36] A. J. Qviller, PhD thesis, University of Oslo, 2012.
[37] J. W. Zuber, F. S. Wells, S. A. Fedoseev, T. H. Johansen, A. B. Rosenfeld, and A. V. Pan, J. Appl. Phys. **123**, 123906 (2018).
[38] J. M. Meckbach, PhD thesis, Karlsruhe Institute for Technology, 2013.
[39] L. E. Helseth, R. W. Hansen, E. I. Il'yashenko, M. Baziljevich, and T. H. Johansen, Phys. Rev. B **64**, 174406 (2001).
[40] P. N. Mikheenko and Yu. E. Kuzovlev, Phys. C **204**, 229 (1993).
[41] Y. B. Kim, C. F. Hempstead, and A. R. Strnad, Phys. Rev. Lett. **9**, 306 (1962).